AIAA-2005-0503
43rd AIAA Aerospace Sciences Meeting & Exhibit
January 10-13, 2005
Reno, NV

DES and Hybrid RANS/LES models for unsteady separated turbulent flow predictions

D. Basu[**], **A. Hamed**[*] **and K. Das**[**]
Department of Aerospace Engineering
University of Cincinnati
Cincinnati, OH 45220-2515

ABSTRACT

This paper proposes two DES (Detached Eddy Simulation) model and one hybrid RANS (Reynolds Averaged Navier-Stokes)/ LES (Large Eddy Simulation) model for the simulations of unsteady separated turbulent flows. The two-equation k-ε based models are implemented in a full 3-D Navier Stokes solver and simulations are carried out using a 3rd order Roe scheme. The predictions of the models are compared for a benchmark problem involving transonic flow over an open cavity and the equivalence between the DES formulations and the hybrid formulation is established. Predicted results for the vorticity, pressure fluctuations, SPL (Sound Pressure level) spectra and different turbulent quantities; such as modeled and resolved TKE (Turbulent Kinetic Energy) profiles, contours and spectra are presented to evaluate various aspects of the proposed models. The numerical results for the SPL spectra are compared with available experimental results and also with the prediction from LES simulations. The grid resolved TKE profiles are also compared with the LES predictions. A comparative study of the CPU time required for the two DES models and the hybrid model is also made.

INTRODUCTION

Most flow predictions for engineering applications at high Reynolds numbers are obtained using the RANS turbulence models. These models yield prediction of useful accuracy in attached flows but fail in complex flow regimes substantially different from the thin shear-layers and attached boundary layers that are used in their calibration. Simulation strategies such as LES are attractive as an alternative for prediction of flow fields where RANS is deficient but carry a prohibitive computational cost for resolving boundary layer turbulence at high Reynolds numbers. This in turn provides a strong incentive for merging these techniques in DES and hybrid RANS-LES approaches.

DES (Detached Eddy Simulations)[1,2,3] was developed as a hybridization technique for realistic simulations of high Reynolds number turbulent flows with massive separation. DES models combined the fine tuned RANS methodology in the attached boundary layers with the power of LES in the shear layers and separated flow regions [4,5,6]. This approach is based on the adoption of a single turbulence model that functions as a sub-grid scale LES model in the separated flow regions where the grid is made fine and nearly isotropic and as a RANS model in attached boundary layers regions. DES predictions of three-dimensional and time-dependent features in massively separated flows are superior to RANS[6].

Spalart et al.[4] first proposed the DES concept based on the original formulation of the Spalart-Allmaras (S-A) one-equation model[7]. Subsequently, Strelets[5], Bush et al.[8], Batten et al.[9], Nichols et al.[10] proposed parallel concepts for two-equation based DES turbulence models. Application of the DES models for a wide variety of problems involving separated flows showed certain degree of success compared to RANS predictions[2,11-15]. In general, these DES models[4-5,8-10] use a transfer function to affect transition from the standard RANS turbulence model to the LES sub-grid type model. The transfer function for the S-A one equation based DES model[4] solely depends on the local grid spacing. In the two-equation based hybrid models[5,8-10], the transfer from RANS to LES regions depends on both local grid spacing and turbulent flow properties.

While DES is based on the adoption of a single turbulence model, another class of hybrid technique

---

**AIAA Fellow, Professor*
***AIAA Student Member, Graduate Student*

relies on two distinct RANS and LES type turbulent models by explicitly dividing the computational domain into RANS and LES regions[16]. However, initialization of the LES fluctuating quantities at the interface presents a challenge because the RANS region deliver Reynolds averaged flow statistics. Baurle et al.[17] proposed another hybrid concept based on k-ω RANS and SGS TKE models. In this case the RANS TKE equations are modified to a form, which is consistent with the SGS TKE equation and a blending function is used. Xiao et al.'s[18] analogous approach is based on a two-equation k-ζ turbulence model. In these approaches, the computational domain is not explicitly divided; instead the model itself uses the RANS and the LES type equations when required depending on the turbulent quantities. Arunajatesan et al.[19] presented a hybrid approach with equations for the sub-grid kinetic energy and the overall turbulent kinetic energy dissipation rate ε.

In the present investigation, two DES formulations and one hybrid formulation are proposed and analyzed. The DES formulations are two-equation k-ε turbulence model based; and rely on the principle of reduction of the eddy viscosity (μ_t) in separated flow regions in proportion to the local resolution. The reduction in the eddy viscosity (μ_t) is achieved through the modifications of either k or ε. The hybrid formulation is based on the combination of the two-equation k-ε turbulence model[20] and a one-equation sub-grid-scale (SGS) model[21]. A blending function allows the SGS TKE equation to be triggered in the separated flow regions and activates the RANS TKE equation in the attached flow regions. The proposed models are evaluated for unsteady separated turbulent flows in transonic cavity.

Transonic cavity flow is dominated by shear layer instability and acoustically generated flow oscillations. It also encompasses both broadband small-scale fluctuations typical of turbulent shear layers, as well as discrete resonance that depend upon cavity geometry and free stream Mach number and the Reynolds number[14,22,23]. The vorticity contours and the iso-surfaces are presented to show the three-dimensionality of the flow field and the fine scale structures. The SPL spectra obtained from the current simulations are compared to the experimental data[24] and also with results obtained from the LES simulations by Rizzetta et al.[25]. The grid resolved turbulent kinetic energy (TKE) profiles are compared with the profiles obtained from the LES simulations[25]. The modeled and the resolved TKE contours are presented to show their distributions in the attached and the separated regions. The grid resolved TKE spectra are also presented to show the energy cascading.

METHODOLOGY

Two DES models are proposed for reducing the eddy viscosity (μ_t) in regions where LES behavior is sought. This is achieved by modification of k and ε that appear in the definition of the eddy viscosity.

DES formulation 1 (DES1)

In this DES formulation, the turbulent kinetic energy dissipation rate (ε) is increased to enable the transition from the RANS to LES type solution. This is achieved through a limiter that is a function of the local turbulent length scale and the local grid dimensions.

$$\varepsilon_{DES} = F_{DES} * [\varepsilon] + (1 - F_{DES}) * [\max(\varepsilon, \frac{k^{3/2}}{C_b * \Delta})] \quad (1)$$

Where,

$$F_{DES} = AINT\ [\min(C_b * \Delta / l_{k-\varepsilon}, 1.0)] \quad (2)$$

In the above expression, AINT is a FORTRAN90 function that truncates the fractional portion of the arguement.

$$\Delta = \max\left(\Delta_{max}, \Delta t * \sqrt{u_i^2}\right) \text{ where, } \sqrt{u_i^2} = \sqrt{u^2 + v^2 + w^2}$$

and

$$\Delta_{max} = \max(\Delta x, \Delta y, \Delta z)$$

In the formulation, C_b is a floating coefficient that has a significant effect on resolved scales and energy cascading[23,26].

DES formulation 2 (DES2)

In this DES formulation, the turbulent kinetic energy (k) is reduced to enable the transition from the RANS to LES type solution. This is achieved through a limiter that is a function of the local turbulent length scale and the local grid dimensions.

$$K_{DES} = F_{DES} * [k] + (1 - F_{DES}) * [\min\{k, (\varepsilon * C_b * \Delta)^{2/3}\}] \quad (3)$$

Where,

$$F_{DES} = AINT\ [\min(C_b * \Delta / l_{k-\varepsilon}, 1.0)] \quad (4)$$

In the above expression, AINT is a FORTRAN90 function that truncates the fractional portion of the argument. Δ and C_b is same as defined in the 1st DES formulation above.

Hybrid Model

The proposed hybrid model is a combination[17] of the RANS two-equation k-ε model[20] and the SGS one - equation model of Yoshizawa and Horiuti.[21] using a blending function.

The RANS TKE equation is given by,

$$\frac{\partial}{\partial t}(\rho k_{RANS}) + \frac{\partial}{\partial x_j}(\rho k_{RANS} U_j) = \frac{\partial}{\partial x_j}\left[\left(\mu + \frac{\mu_{t_{RANS}}}{\sigma_{k_1}}\right)\frac{\partial k_{RANS}}{\partial x_j}\right] + (P_k)_{RANS} - \rho(\varepsilon + \varepsilon_c) + L_K \quad (5)$$

where, $\varepsilon_c = \gamma M_t^2 \varepsilon$ and $M_t = \sqrt{\frac{2k_{RANS}}{a^2}}$

The SGS TKE equation is given by,

$$\frac{\partial}{\partial t}(\rho k_{sgs}) + \frac{\partial}{\partial x_j}(\rho k_{sgs} U_j) = \frac{\partial}{\partial x_j}\left[\left(\mu + \frac{\mu_{t_{sgs}}}{\sigma_{k_2}}\right)\frac{\partial k_{sgs}}{\partial x_j}\right] + P_{k_{sgs}} - \rho C_d \frac{(k_{sgs})^{\frac{3}{2}}}{\Delta} \quad (6)$$

The combined equation is given by

$$\frac{\partial}{\partial t}(\rho k) + \frac{\partial}{\partial x_j} = \frac{\partial}{\partial x_j}\left[\left(\mu + \frac{\mu_t}{\sigma_k}\right)\frac{\partial k}{\partial x_j}\right] + P_k - \rho\left(1 + \gamma M_t^2\right) * \left[F * \varepsilon + (1-F) * C_d \frac{(k)^{\frac{3}{2}}}{\Delta}\right] + F * L_k \quad (7)$$

where,

$$k = F * k_{RANS} + (1-F) * k_{SGS} \quad (8)$$

$$\mu_{t_{RANS}} = C_{\mu 1} * f_\mu * R_{et} * \mu \text{ and } \mu_{t_{SGS}} = C_{\mu 2} * \rho * \sqrt{k_{sgs}} * \Delta$$

$$\mu_{t_{SGS}} = \min[\mu_{t_{RANS}}, \mu_{t_{SGS}}]$$

The hybrid eddy viscosity is given by,

$$\mu_{t_{hybrid}} = F * \mu_{t_{RANS}} + (1-F) * \mu_{t_{SGS}} \text{ ; and } \frac{1}{\sigma_k} = \frac{(F)}{\sigma_{k1}} + \frac{(1-F)}{\sigma_{k2}}$$

where,

F is the blending function; and $\sigma_{k1}, \sigma_{k2}, C_{\mu 1}, C_{\mu 2}$ are parent model constants.

In the above equation, $\sigma_{k1} = 1.0$, $\sigma_{k2} = 1.0$, $C_{\mu 1} = 0.09$ and $C_{\mu 2} = 0.008232$ and $C_d = 1.5$[17,21,27]. The blending function F is given by

$$F = \frac{1 + \tanh[2\pi(f_d - 0.5)]}{2.0} \quad (9)$$

$$\text{where, } f_d = \text{AINT}\left[\min\left(\frac{C_b * \Delta}{l_{k-\varepsilon}}, 1.0\right)\right] \quad (10)$$

Essentially the RANS TKE equation is reformulated in such a way that it is consistent with and resembles the SGS TKE equation[21]. The function AINT, coefficient C_b and Δ are the same quantities as defined in the DES formulations.

NUMERICS

The governing equations for the present analysis are the full unsteady, three-dimensional compressible Navier-Stokes equations written in strong conservation-law form. They are numerically solved employing the implicit, approximate-factorization, Beam-Warming algorithm[28] along with the diagonal form of Pullinam and Chaussee[29]. Newton subiterations are used to improve temporal accuracy and stability properties of the algorithm. The aforementioned features of the numerical algorithm are embodied in a parallel version of the time accurate three-dimensional solver FDL3DI, originally developed at AFRL[30,31]. In the Chimera based parallelization strategy[32] used in the solver, the computational domain is decomposed into a number of overlapped sub-domains as shown in figure 1[32]. An automated pre-processor PEGSUS[33] is used to determine the domain connectivity and interpolation function between the decomposed zones. In the solution process, each sub-domain is assigned to a separate processor and communication between them is accomplished through the interpolation points in the overlapped region by explicit message passing using MPI libraries. The solver has been validated and proved to be efficient and reliable for a wide range of high speed and low speed; steady and unsteady problems[25,32,34-36].

For the present research, the two-equation k-ε based DES models and a hybrid RANS-LES model have been implemented in the solver within the present computational framework. The 3rd order Roe scheme is used for the spatial discretization for both the flow and the turbulent equations. The time integration is carried out using the implicit Beam-Warming scheme with three subiterations for each time step.

The floating coefficient C_b mentioned in the DES models as well as the definition of the blending function has been used in most of the prior DES formulations[4,5,8-10]. Essentially the desired value of this floating coefficient should give a spectrum that avoids the build-up of the high-frequency oscillations and the suppression of resolvable eddies. Based on calibration of homogeneous turbulence, this value was suggested at 0.61. However, previous investigations[14,23] by the current authors for the cavity flow determined that C_b should be between 0.1 and 0.5 to yield adequate levels of resolved turbulent energy and capture the resolved scales. They found that a value of 0.1 for the C_b gives the best result in terms of the SPL spectra and the resolved flowfield. Mani[26] also carried out DES simulations of jet flows

with different C_b values and found that C_b should be between 0.1 and 0.5. For the present formulations, the value of C_b is kept at 0.1.

The transonic cavity problem, chosen for the present analysis has been earlier analyzed by the current authors[23] to determine the effects of the computational grid and C_b on the SPL spectra and the TKE. The analysis found out that the computed SPL in general, and the peak SPL at the dominant frequency in particular are very sensitive to grid resolution and also C_b. Rizzetta et al.[25] carried out LES analysis for the same cavity configuration at a Reynolds number of 0.12×10^6/ft, using the dynamic SGS model with a 4th order compact pade-type scheme. The LES simulations were carried out using 25×10^6 grid points in a massive parallel computational platform with 254 processors and required pulsating flow to accomplish transition upstream of the cavity front bulkhead.

The cavity geometry has a L/D (length-to-depth) ratio of 5.0 and a W/D (width-to-depth) ratio of 0.5. The computed results are compared to the experimental data of DERA[24] which were obtained at a Reynolds number of 4.336×10^6/ft and a transonic Mach number of 1.19. To optimize the use of available computational resources while maintaining a fully turbulent boundary layer at the front bulkhead cavity lip, the present simulations were performed at a Reynolds number of 0.60×10^6/ft, which is $(1/7)^{th}$ the value of the experimental Reynolds number and the same experimental Mach number of 1.19. The solution domain for the cavity is shown in figure 2. Free stream conditions were set for the supersonic inflow and first order extrapolation was applied at the upper boundary, which was at 9D above the cavity opening. First order extrapolation was also applied at the downstream boundary, 4.5D behind the rear bulkhead. Periodic boundary conditions were applied in the span-wise direction. The upstream plate length was 4.5D in order to maintain the incoming boundary layer thickness δ at 10% of the cavity depth D, at the simulated Reynolds number. The computational grid consists of 300×120×80 grid points in the stream-wise, wall normal and span-wise direction respectively. Within the cavity, there are 160 grids in the axial direction, 60 grid points in the wall normal direction and 80 grid points in the spanwise direction. It is based on the prior assessment[23] of the current authors regarding the effect of the grid resolution on the SPL spectra and the TKE cascading. The grid is packed near the walls, with a minimum wall normal grid spacing (Δy) of 1×10^{-4}D. This corresponds to an y^+ of 1.0 for the first grid point. The grid is clustered in the wall normal direction using hyperbolic tangent stretching function with 20 grid points within the boundary layer upstream of the cavity. Within the cavity, the minimum Δy corresponds to an y^+ of 10. In the stream-wise direction within the cavity, the minimum Δx corresponds to an x^+ of 50. In the span-wise direction, constant grid spacing is used which results in a z^+ of 63.

The solution domain is decomposed into twelve overlapping zones in the stream-wise direction and the normal direction for parallel computation with a five-point overlap between the zones. Parallel computations for the overlapping zones for cavity were performed using Itanium cluster machines and exclusive message passing with MPI libraries. The zones were constructed in such a way that the load sharing among the processors were nearly equal.

The DES and hybrid RANS/LES simulations were initiated in the unsteady mode and continued over 120,000 constant time-steps of 2.5×10^{-7} seconds. It took 40,000 time steps to purge out the transient flow and establish resonance and the remaining 80,000 time steps to capture 12 cycles in order to have sufficient data for statistical analysis. The sound pressure level (SPL) and the turbulent kinetic energy (TKE) spectra for the cavity simulations are computed for all cases based on 65536 sample points.

RESULTS AND DISCUSSIONS

The pressure fluctuations for all three models are presented. The associated SPL spectra are compared with available experimental results[24] and with LES simulations[25]. Grid resolved turbulent kinetic energy (TKE) profiles are also compared with the LES simulations. Contours and iso-surfaces of the vorticity field are presented to show the fine scale structures and three-dimensionality of the flowfield. Spectra for the resolved TKE are presented to show the energy cascading.

The computed boundary layer profile upstream of the cavity lip is compared to the well-known formula of Spalding[37] in figure 3 for the two DES models and the hybrid formulation. The results indicate that the computed boundary layer is fully turbulent for all three cases and is in agreement with Spalding's formula.

Figure 4 shows the instantaneous contours of the span-wise vorticity at the cavity mid-span for the three models (DES1, DES2 and the Hybrid model) from the present simulations. The instantaneous prediction from the 3-D URANS simulations is also

shown for reference. The roll up of the vortex and the impingement of the shear layer at the rear bulkhead can be seen in figure 4. The figures also indicate the formation of eddies that are smaller than the shed vortex within the cavity. It can be seen that all the models resolve significant small scales within the separated flow region inside the cavity. It can be clearly observed that the URANS simulations fail to predict any fine scale structures within the cavity and in the shear layer. The location of the oblique shock at the upstream and at the downstream locations can be seen as well.

Figure 5 presents the instantaneous iso-surfaces of the spanwise component of the quantity Q (Q_z) to show the three-dimensionality of the flowfield, the formation of the separated eddies within the cavity and also the evolution of the vortical structures. The Q criterion is proposed by Hunt et al[38] and is used here to show the coherent vortices downstream of the cavity forward bulkhead. It clearly indicates the formation of the Kelvin-Helmholtz instabilities as the shear layer passes over the cavity lip, the gradual roll-up/lifting of the shear layer, the breakdown of the vortex as it is convected downstream and the associated formation of separated eddies. It can be observed that at the upstream region, the vortex sheet is essentially two-dimensional in nature. After separating from the step and expanding into the separated region, the 2-D Kelvin-Helmholtz structures develop and eventually break down into three-dimensional turbulent structures. Similar observations were also made by Dubief and Delcayre[39] in their LES simulations of BFS flow.

Figure 6 shows the iso-surfaces of the axial component of the quantity Q (Q_x). The axial component shows the three-dimensionality of the flow field in more details. It is evident in figure 6 that Q_x is present in significant amount only in the separated regions and this clearly shows that the 3-D nature of the flow-field within the cavity. As the vortex is convected downstream, the three-dimensionality of the flowfield becomes more prominent and the subsequent stretching and pairing of the vortex structures increases.

Figure 7 shows the computed pressure fluctuations history at two streamwise locations on the cavity floor (Y/D = 0.0) near the front (X/L = 0.2) and rear (X/L = 0.8) bulkheads respectively for the three turbulence models. The amplitude at X/L = 0.8 is higher compared to the amplitude at X/L = 0.2. The amplitudes for the pressure fluctuations predicted by the DES2 model and the hybrid model are slightly higher than the amplitude predicted by the DES1 model.

Figure 8 shows the corresponding sound pressure level (SPL) spectra at the two streamwise locations (X/L = 0.2 and X/L = 0.8) on the cavity floor (Y/D = 0.0) and are compared to the experimental data[24]. The SPL spectra were obtained by transforming the pressure-time signal into the frequency domain using fast Fourier transform (FFT). The peak SPL predicted by the current simulations, the LES simulations[25] and that for the available experimental data[24] are shown in the tables below.

Cases	Peak SPL at X/L = 0.2 (dB)	Difference with experimental value (dB)
DES1	152	3
DES2	154	1
Hybrid	154	1
LES	152	3
Experiment	**155**	

Cases	Peak SPL at X/L = 0.8 (dB)	Difference with experimental value (dB)
DES1	162	3
DES2	163	2
Hybrid	163	2
LES	164	1
Experiment	**165**	

It can be seen that all the current simulations predict the dominant frequencies in close agreement with the experimental data. All three models predict the dominant modes including the first mode that occurs at around 220 Hz. Among the three models, the DES1 model and the hybrid model predict the 1st mode peak SPL amplitude in closer agreement with the experimental data. There is however some difference between the peak SPL values of the highest dominant mode (2nd mode) in the predicted solutions and the experimental results both at X/L = 0.2 and at X/L = 0.8. Among the three models, the DES2 model and the hybrid model predicts the 2nd mode peak SPL value closest to the experimental data. The predictions from all three models over predict the experimental SPL values at higher frequencies especially at X/L = 0.8.

Figure 9 shows the comparison of the SPL spectra at the above locations on the cavity floor from the current predictions with the LES simulations. It can be seen that the overall trend of the SPL spectra

matches well with the LES predictions. The LES simulations were carried out at a Reynolds number of 0.12×10^6/ft; which was 1/5th of the Reynolds number at which the current simulations are carried out. The peak SPL values from all the models are comparable to the LES predictions. The predictions from all three models follow the LES spectra very closely at the higher frequencies especially for the DES2 and the hybrid model, but the spectra from the DES1 model slightly over-predicts the LES spectra values especially at X/L = 0.8.

Figure 10 shows the contours for the time-mean spanwise averaged modeled TKE for all three models. It can be observed that in the attached boundary layer regions in the upstream and downstream of the cavity there is significant amount of modeled TKE. It can be observed that the modeled TKE is present in significant amount only in the attached boundary layer regions, which is governed by the RANS model. Inside the cavity, the magnitude of the modeled TKE is much less for all three cases.

Figure 11 shows the contours for the time-mean spanwise averaged grid resolved TKE for all three models. The resolved TKE is obtained from the velocity fluctuations (u', v', w') in the three directions. It clearly shows that in the separated LES type regions within the cavity, the DES models as well as the hybrid model predicts significant amount of resolved TKE.

Figure 12 show the time-mean spanwise averaged grid resolved turbulent kinetic energy (TKE) profiles across the cavity shear layer (y/D=1.0) at three streamwise locations. y/D = 1.0 represents the cavity opening. The predictions from all the models are compared to the prediction from the LES simulations[25]. It can be seen that all the models predict the grid resolved TKE inside the cavity between the regions y/D = 0.25 to y/D = 1.5 in reasonable agreement with the LES simulations. The profile at X/L = 0.2 matches best with the LES simulations throughout (y/D = 0.0 to y/D = 2.0). However, at the two downstream locations (X/L = 0.5 and X/L = 0.8) near the bottom wall of the cavity (between y/D = 0.0 to y/D = 0.2), the current simulations under predict the resolved TKE compared to the LES simulations. This can be attributed to the fact that for the LES simulations there were 121 grids employed within the cavity in the wall normal direction primarily to resolve the near wall very fine eddies. However, in the present simulations, 60 grids were employed in the wall normal direction. Hence in the near wall region, current simulations were unable to predict the same level of grid resolved TKE compared to the LES simulations. But in the shear layer region across the cavity opening, the current simulations match reasonably well with the LES values. Among the three models, the predictions from the DES1 model and the hybrid model match more closely with the LES simulations. The prediction from the DES2 model is lower than the prediction from the other two models and the LES simulations.

Figure 13 shows the profiles of TKE dissipation rate (ε) and the quantity $k^{3/2}/(C_b*\Delta)$ [Referred as DES dissipation rate] across the cavity shear layer at three separate axial locations. It can be seen that at X/L = 0.2, the two quantities are almost of the same magnitude within the cavity but the DES dissipation rate has a much higher value compared to ε in the shear layer region of the cavity opening. Progressing further downstream along the cavity one can see that the DES dissipation rate is much higher than ε in the separated regions within the cavity and also in the shear layer region at the cavity opening.

Figure 14 shows the span-wise averaged grid resolved TKE spectra at two streamwise locations (X/L = 0.2 and X/L = 0.8). The two positions are located within the turbulent shear layer at the cavity opening (y/D = 1.0). The –5/3 slope of Kolmogorov is also in the figure for reference. It can be observed that there is a significant reduction in the magnitude of the energy spectrum E(k) at higher frequency for all the three models; which indicates that all the models resolve the fine scale structures. However, the 2nd DES model (DES2) has higher amplitude compared to DES1 and the hybrid model and a significantly more prominent peak at the dominant frequencies. This trend can be observed at both the streamwise locations.

CONCLUSIONS

This paper presents two DES models and one-hybrid RANS/LES model for simulation of turbulent flows at high Reynolds numbers. The models are applied to transonic flow over an open cavity. Simulated results show that the models are successfully able to capture the flow features in the separated flow regions, including three-dimensionality, the fine scale structures and the unsteady vortex shedding. The computed results from all three models are compared with available experimental data and also with LES simulations. Predicted SPL spectra compare favorably with both the experimental data as well as the LES results. Among the three models, the DES2 model and the hybrid model performs better with respect to the prediction of the peak SPL. The grid

resolved TKE in the shear layer region are consistent with the LES results. Discrepancies in the near wall region can be attributed to insufficient grid resolution in the near wall RANS region compared to the LES grid. There is significant reduction in the spectrum at higher frequencies for all the models. However, the spectra from DES2 has higher amplitude at dominant frequencies compared to DES1 and the hybrid model. The hybrid model takes a slightly higher CPU time than the other two DES models. This paper shows that the predictions from the DES models and the hybrid model with an order of magnitude less grid (compared to LES) are comparable to the LES predictions with an acceptable level of accuracy.

ACKNOWLEDGEMENTS

The authors would like to thank Dr. Philip Morgan at WPAFB and Prof. Karen Tomko at UC for many useful suggestions regarding the code FDL3DI; Dr. Donald Rizzetta at WPAFB for providing the LES simulation results and Dr. Robert Baurle at NASA Langley for his valuable suggestions regarding the hybrid model. Majority of the computations were carried out in the Itanium 2 Cluster at the Ohio Supercomputer Center (OSC) and in the Linux cluster at UC set up by Mr. Robert Ogden.

REFERENCES

1. Spalart, P. R., "Strategies for Turbulence Modeling and Simulations," 2000, International Journal of Heat and Fluid Flow, Vo. 21, pp. 252-263.
2. Hamed, A., Basu, D., and Das, K., "Detached Eddy Simulations of Supersonic Flow over Cavity," 2003, 41st AIAA Aerospace Sciences Meeting and Exhibit, Reno, Nevada, AIAA - 2003-0549.
3. Sinha, N., Dash, S. M., Chidambaram, N. and Findlay, D., "A Perspective on the Simulation of Cavity Aeroacosutics", 1998, AIAA-98-0286.
4. Spalart, P. R., Jou, W. H., Strelets, M., and Allmaras, S. R., "Comments on the Feasibility of LES for Wings, and on a Hybrid RANS/LES Approach," 2001, First AFOSR International Conference on DNS/LES, Ruston, Louisiana, USA.
5. Strelets, M., "Detached Eddy Simulation of Massively Separated Flows", 2001, 39th AIAA Aerospace Sciences Meeting and Exhibit, AIAA-2001-0879.
6. Krishnan, V., Squires, K. D., Forsythe, J. R., "Prediction of separated flow characteristics over a hump using RANS and DES", 2004, AIAA-2004-2224.
7. Spalart, P. R., and Allmaras, S. R., " A one-equation turbulence model for aerodynamic flows", La Rech. A'reospatiale, 1994, Vol. 1, pp. 5-21.
8. Bush, R. H., and Mani, Mori, "A two-equation large eddy stress model for high sub-grid shear", 2001, 31st AIAA Computational Fluid Dynamics Conference, AIAA-2001-2561
9. Batten, P., Goldberg, U., and Chakravarthy, S., "LNS – An approach towards embedded LES", 2002, 40th AIAA Aerospace Sciences Meeting and Exhibit, AIAA-2002-0427.
10. Nichols, R. H., and Nelson, C. C., "Application of Hybrid RANS/LES Turbulence models", 2003, 41st AIAA Aerospace Sciences Meeting and Exhibit, Reno, Nevada, AIAA 2003-0083.
11. Travin, A., Shur, M., Strelets, M. and Spalart, P. R., "Detached-Eddy Simulations Past a Circular Cylinder," 1999, Flow Turbulence and Combustion, Vol. 63, pp. 293-313.
12. Constantinescu, G., Chapelet, M., Squires, K., "Turbulence Modeling Applied to Flow over a Sphere," 2003, AIAA Journal, Vol. 41, No. 9, pp. 1733-1742.
13. Hedges, L. S., Travin, A. K. and Spalart, P. R., "Detached-Eddy Simulations Over a Simplified Landing Gear," 2002, Journal of Fluids Engineering, Transaction of ASME, Vol. 124, No. 2, pp. 413-423.
14. Hamed, A., Basu, D., and Das, K., "Effect of Reynolds Number on the Unsteady Flow and Acoustic Fields of a Supersonic Cavity," 2003, Proceedings of FEDSM '03, 4th ASME-JSME Joint Fluids Engineering Conference, Honolulu, HI, Jul 6-11, FEDSM2003-45473.
15. Forsythe, J. R., Squires, K. D., Wurtzler, K. E., and Spalart, P. R., "Detached-Eddy Simulation of the F-15E at High Alpha", 2004, Journal of Aircraft, Vol. 41, No. 2, pp. 193-200.
16. Georgiadis, N. J., Alexander, J. I. D., and Roshotko, E., "Hybrid Reynolds-Averaged Navier-Stokes/Large-Eddy Simulations of Supersonic Turbulent Mixing", 2003, AIAA Journal, Vol. 41, No. 2, pp. 218-229
17. Baurle, R. A., Tam, C. J., Edwards, J. R., and Hassan, H. A., "Hybrid Simulation Approach for Cavity Flows: Blending, Algorithm, and Boundary Treatment Issues", 2003, AIAA Journal, Vol. 41, No. 8, pp. 1463-1480.
18. Xiao, Xudong, Edwards, J. R., Hassan, H. A., and Baurle, R. A., "Inflow Boundary Conditions for Hybrid Large Eddy/ Reynolds Averaged Navier-Stokes Simulations", 2003, AIAA Journal, Vol. 41, No. 8, pp. 1481-1489.
19. Arunajatesan, S. and Sinha, N., " Hybrid RANS-LES modeling for cavity aeroacoustic

predictions", 2003, International Journal of Aeroacoustics, Vol. 2, No. 1, pp. 65-93.
20. Gerolymos, G. A., "Implicit Multiple grid solution of the compressible Navier-Stokes equations using k-ε turbulence closure", 1990, AIAA Journal, Vol. 28, No. 10, pp. 1707-1717.
21. Yoshizawa, A., and Horiuti, K., "A Statistically Derived Subgrid Scale Kinetic Energy Model for the Large-Eddy Simulation of Turbulent Flows", 1985, Journal of the Physical Society of Japan, Vol. 54, No. 8, pp. 2834-2839.
22. Hamed, A., Basu, D., Mohamed, A. and Das, K., "Direct Numerical Simulations of Unsteady Flow over Cavity," 2001, Proceedings 3rd AFOSR International Conference on DNS/LES (TAICDL), Arlington, Texas.
23. Hamed, A., Basu, D., and Das, K., "Assessment of Hybrid Turbulence Models for Unsteady High Speed Separated Flow Predictions", 2004, 42nd AIAA Aerospace Sciences Meeting and Exhibit, Reno, Nevada, AIAA -2004-0684.
24. Ross, J. et al., "DERA Bedford Internal Report," 1998, MSSA CR980744/1.0.
25. Rizzetta, D. P. and Visbal, M. R., "Large-Eddy Simulation of Supersonic Cavity Flow Fields Including Flow Control," 2003, AIAA Journal, Vol. 41, No. 8, pp. 1452-1462.
26. Mani, M., "Hybrid Turbulence Models for Unsteady Simulation of Jet Flows," 2004, Journal of Aircraft, Vol. 41, No. 1, pp. 110-118.
27. Baurle, R. A., 2004, Private Communications.
28. Beam, R., and Warming, R., "An Implicit Factored Scheme for the Compressible Navier-Stokes Equations," 1978, AIAA Journal, Vol. 16, No. 4, pp. 393-402.
29. Pullinam, T., and Chaussee, D., "A Diagonal Form of an Implicit Approximate-Factorization Algorithm," 1981, Journal of Computational Physics, Vol. 39, No. 2, pp. 347-363.
30. Gaitonde, D., and Visbal, M. R., "High-Order Schemes for Navier-Stokes Equations: Algorithm and Implementation into FL3DI", 1998, AFRL-VA-TR-1998-3060.
31. Morgan, P., Visbal, M., and Rizzetta, D., "A Parallel High-Order Flow Solver for LES and DNS", 2002, 32nd AIAA Fluid Dynamics Conference, AIAA-2002-3123.
32. Morgan, P. E., Visbal, M. R., and Tomko, K., "Chimera-Based Parallelization of an Implicit Navier-Stokes Solver with Applications", 2001, 39th Aerospace Sciences Meeting & Exhibit, Reno, NV, January 2001, AIAA Paper 2001-1088.
33. Suhs, N. E., Rogers, S. E., and Dietz, W. E., "PEGASUS 5: An Automated Pre-processor for Overset-Grid CFD", June 2002, AIAA Paper 2002-3186, AIAA Fluid Dynamics Conference, St. Louis, MO.
34. Visbal, M. R. and Gaitonde, D., "Direct Numerical Simulation of a Forced Transitional Plane Wall Jet", 1998, AIAA 98-2643.
35. Visbal, M. and Rizzetta, D., "Large-Eddy Simulation on Curvilinear Grids Using Compact Differencing and Filtering Schemes", 2002, ASME Journal of Fluids Engineering, Vol. 124, No. 4, pp. 836-847.
36. Rizzetta, D. P., and Visbal, M. R., 2001, "Large Eddy Simulation of Supersonic Compression-Ramp Flows", AIAA-2001-2858.
37. Spalding, D.B., "A single formula for the law of the wall", 1961, Journal of Applied Mechanics, Vol. 28, pp. 455.
38. Hunt, J. C. R., Wray, A. A., and Moin, P., "Eddies, stream, and convergence zones in turbulent flows", 1988, Proceedings of the 1988 Summer Program, Report CTR-S88, Center for Turbulence Research, pp. 193-208.
39. Dubief, Y., and Delcayre, F., "On coherent-vortex identification in turbulence", 2000, Journal of Turbulence, Vol. 1, Issue 1, pp. 1-22.

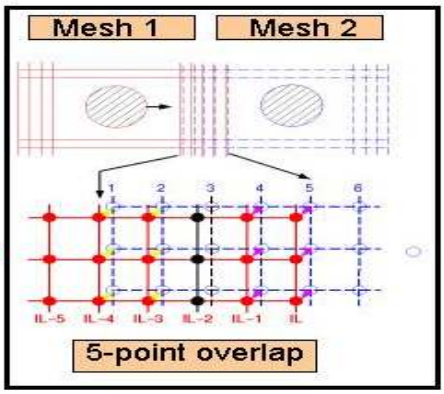

Figure 1 Schematic of the domain connectivity for the parallel solver (32)

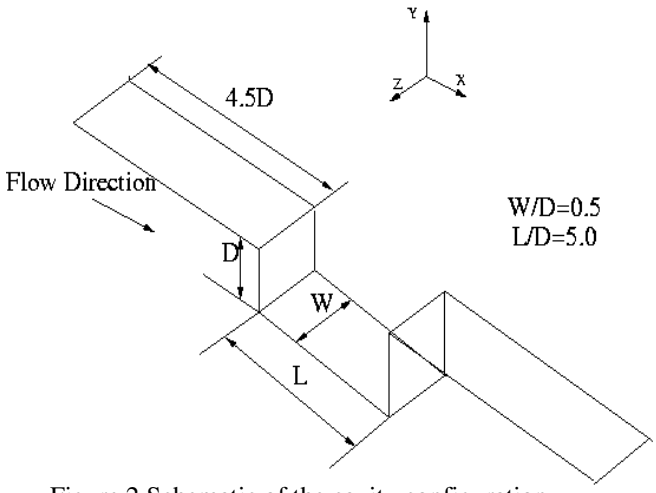

Figure 2 Schematic of the cavity configuration

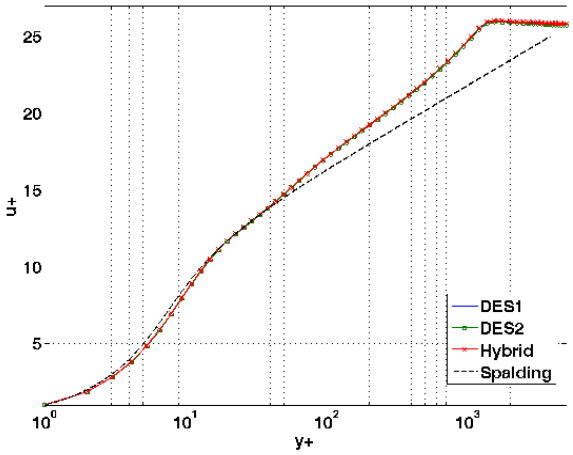

Figure 3 Streamwise velocity profiles at the upstream region of the cavity

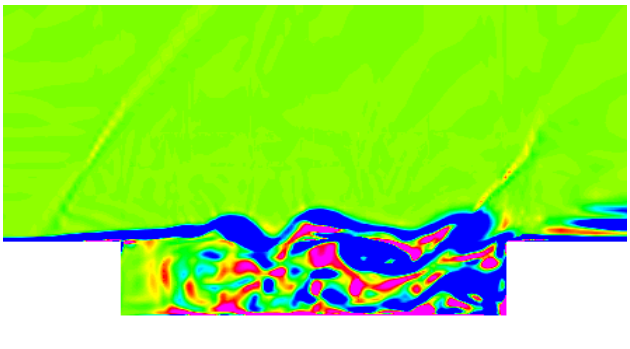

DES1

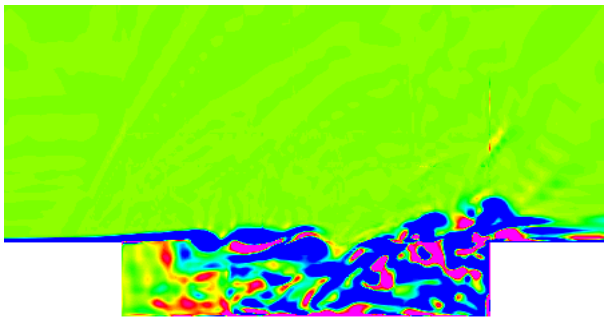

DES2

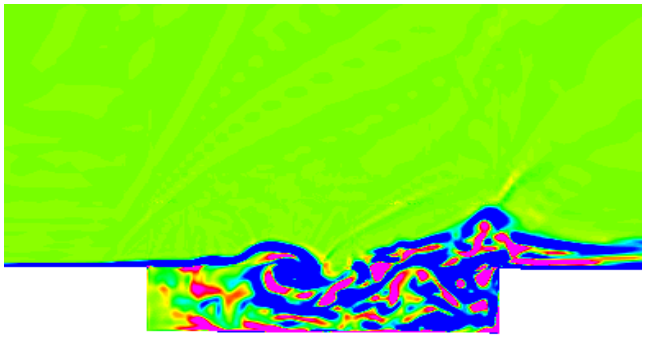

Hybrid

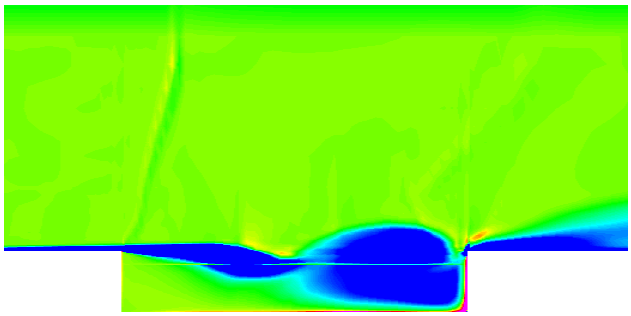

URANS

Figure 4 Span-wise vorticity contours at the cavity mid-span

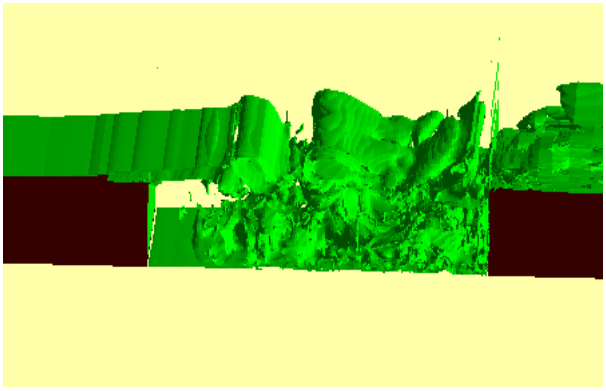

DES1

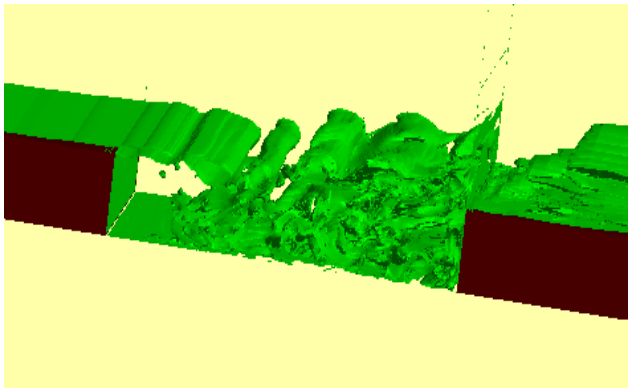

DES2

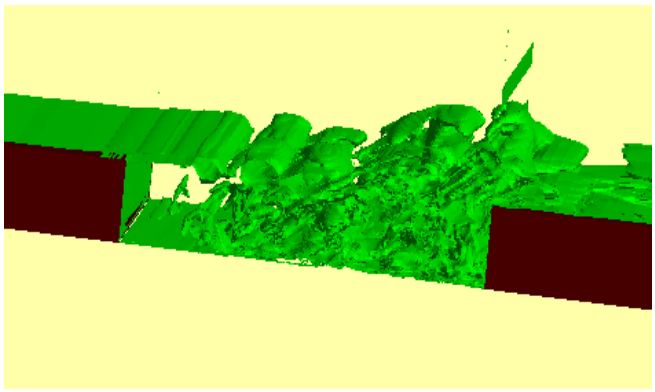

Hybrid

Figure 5 Iso-surfaces of the span-wise component of Q (Q_z) for the transonic cavity flow

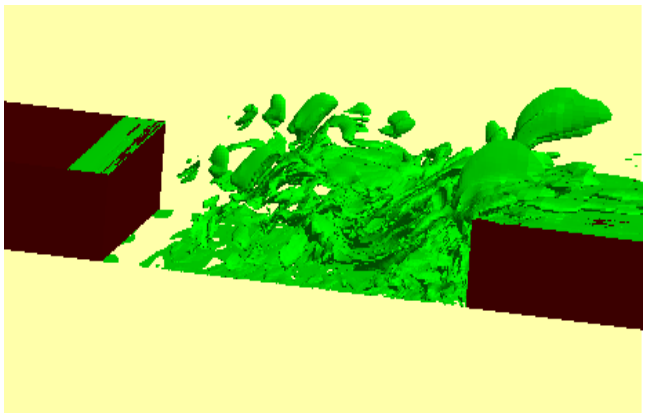

DES1

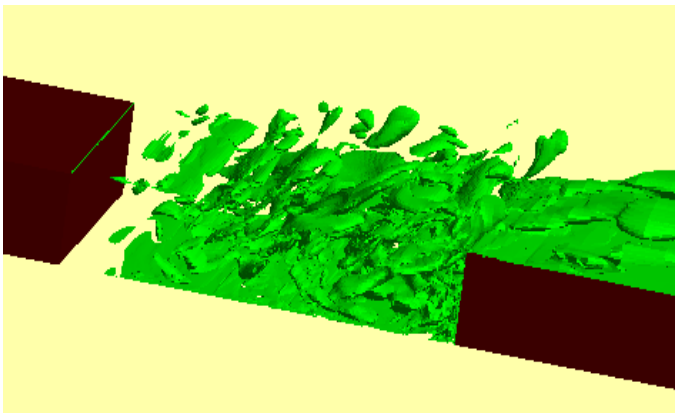

DES2

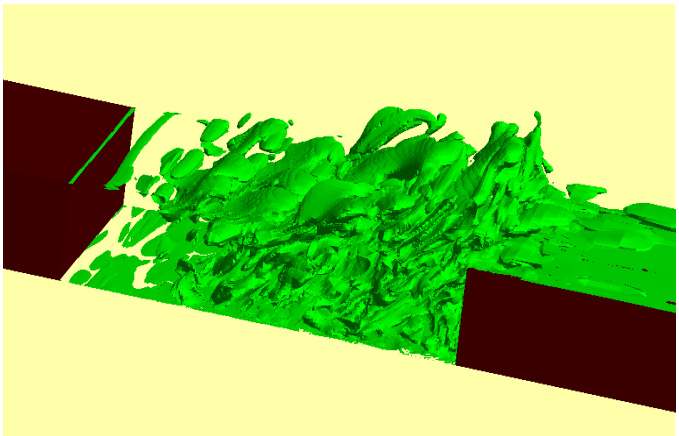

Hybrid

Figure 6 Iso-surfaces of the axial component of Q (Q_x) for the transonic cavity flow

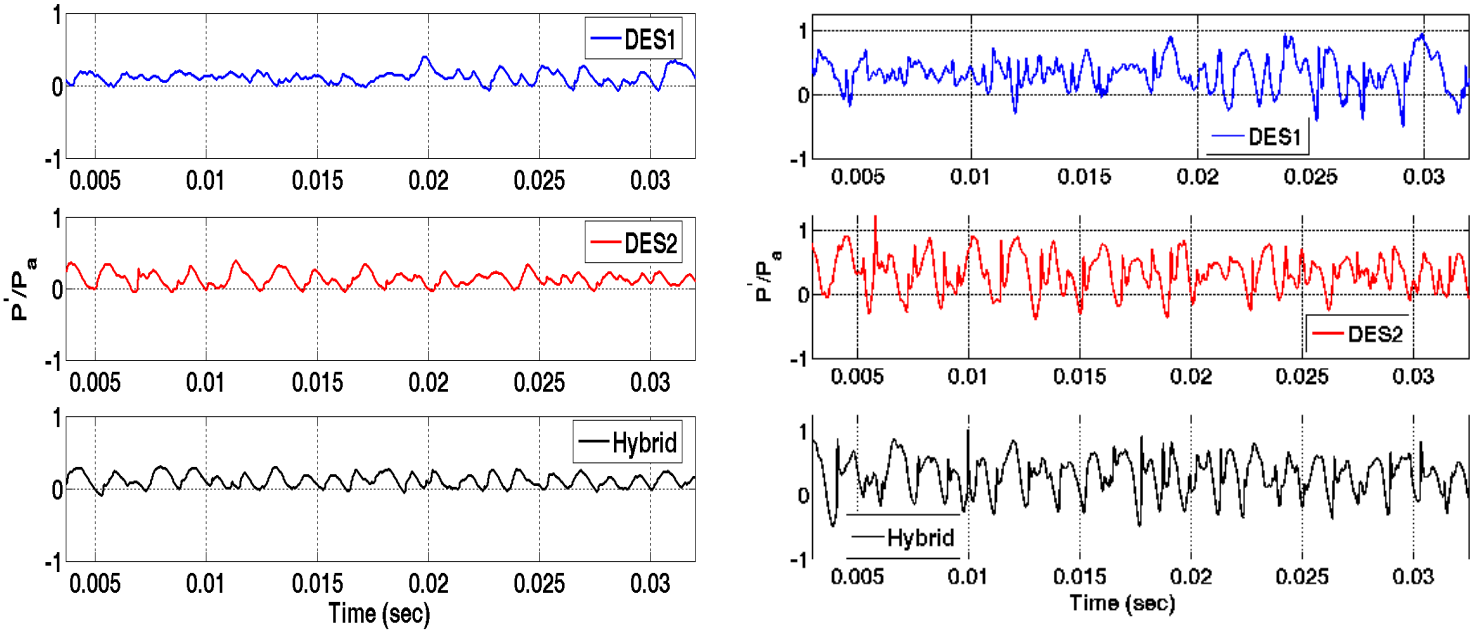

X/L = 0.2 X/L = 0.8

Figure 7 Time history of span-wise averaged fluctuating pressure on the cavity floor (Y/D = 0.0)

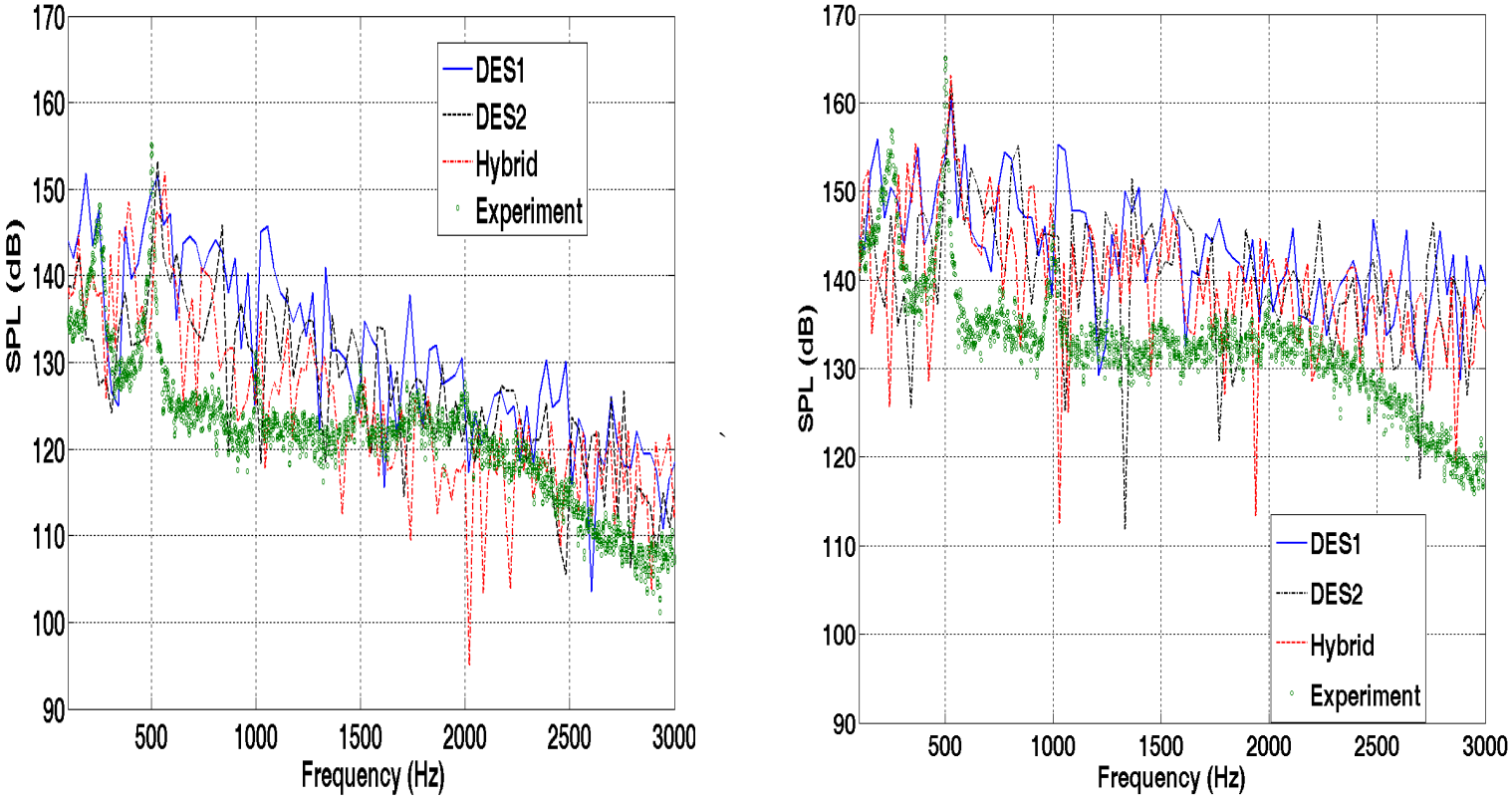

X/L = 0.2 X/L = 0.8

Figure 8 Span-wise averaged fluctuating pressure frequency spectra on the cavity floor (Y/D = 0.0): Comparison with experimental data (24)

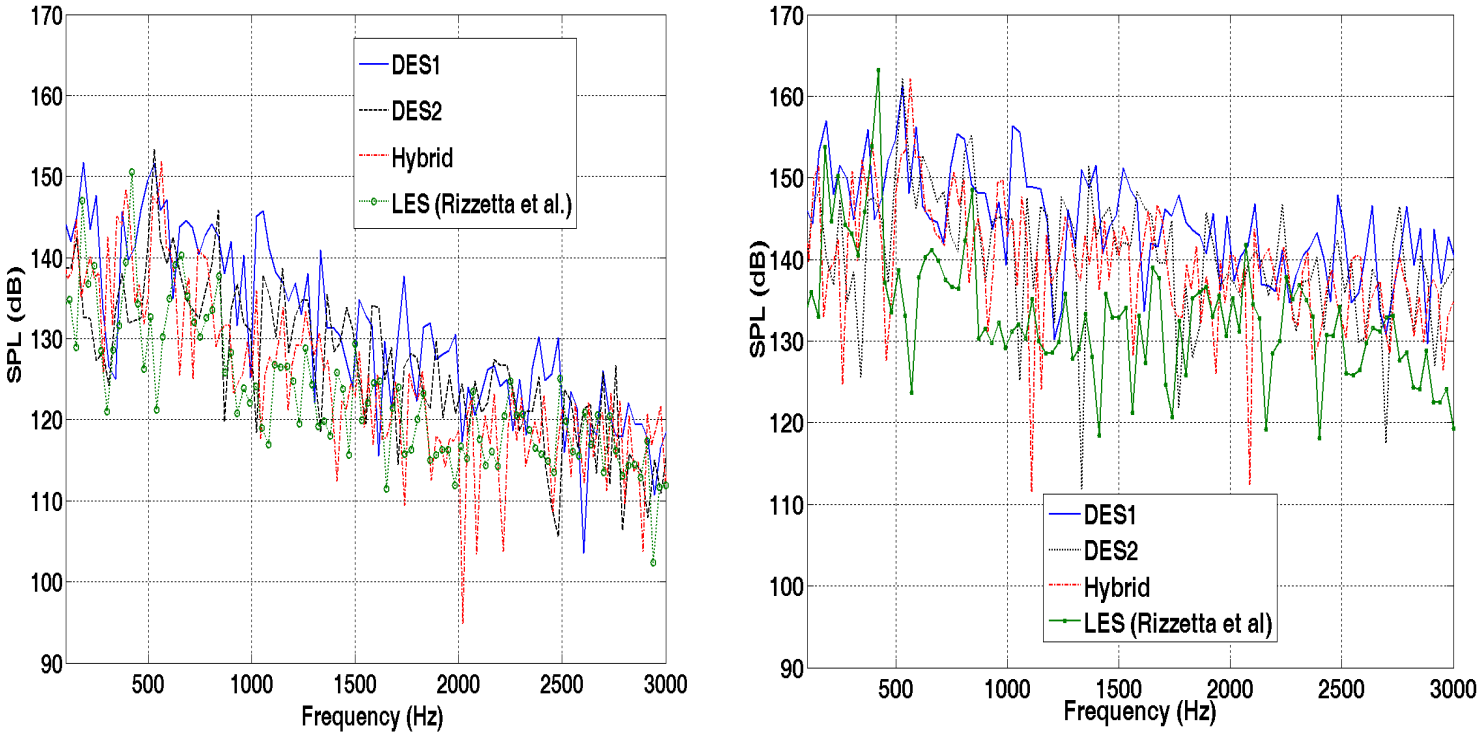

X/L = 0.2 X/L = 0.8

Figure 9 Span-wise averaged fluctuating pressure frequency spectra on the cavity floor (Y/D = 0.0): Comparison with LES Simulations (25)

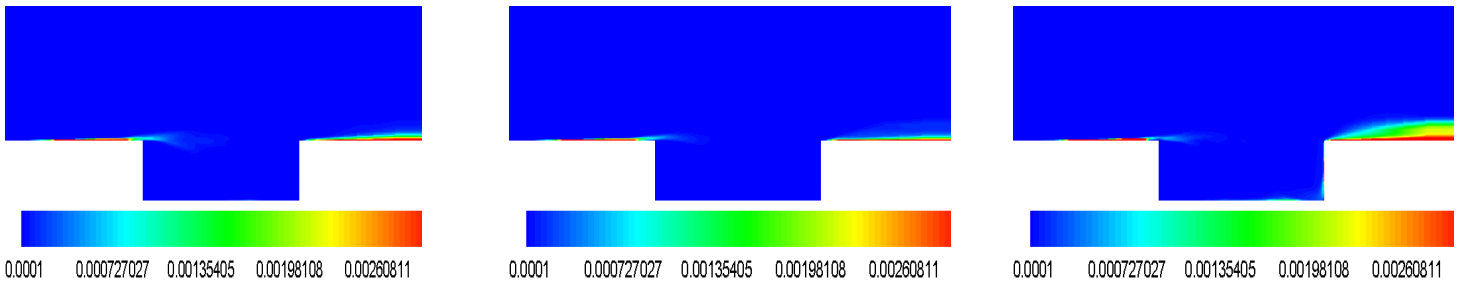

DES1 DES2 Hybrid

Figure 10 Spanwise averaged time-mean modeled turbulent kinetic energy contours

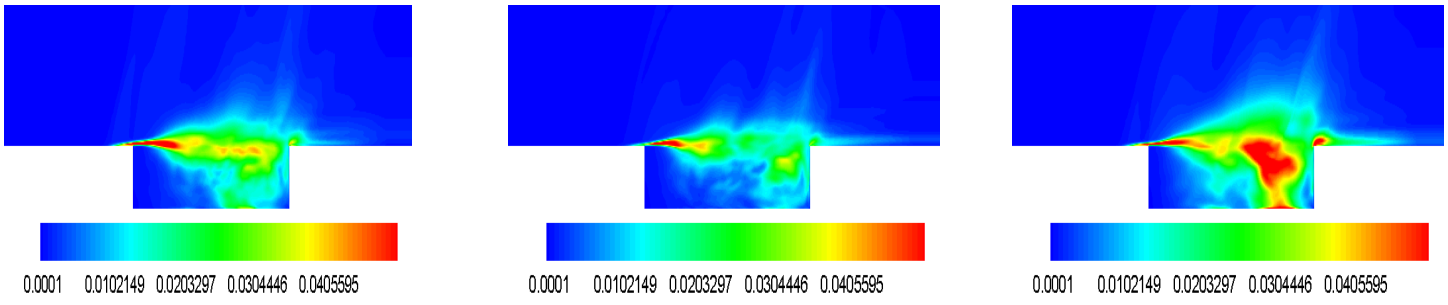

DES1 DES2 Hybrid

Figure 11 Spanwise averaged time-mean grid resolved turbulent kinetic energy contours

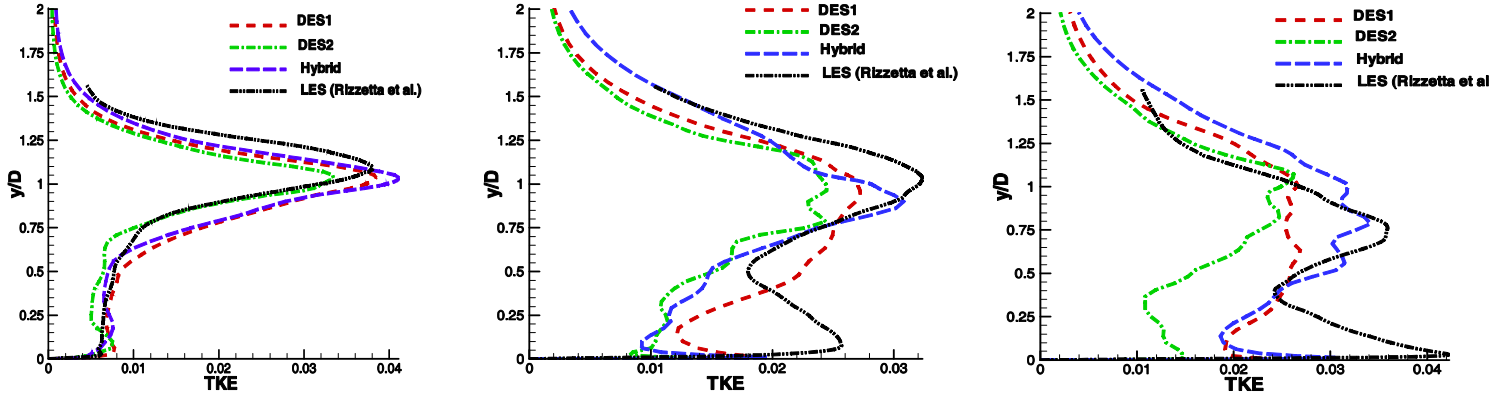

X/L = 0.2 X/L = 0.5 X/L = 0.8

Figure 12 Spanwise averaged time-mean grid resolved turbulent kinetic energy profiles

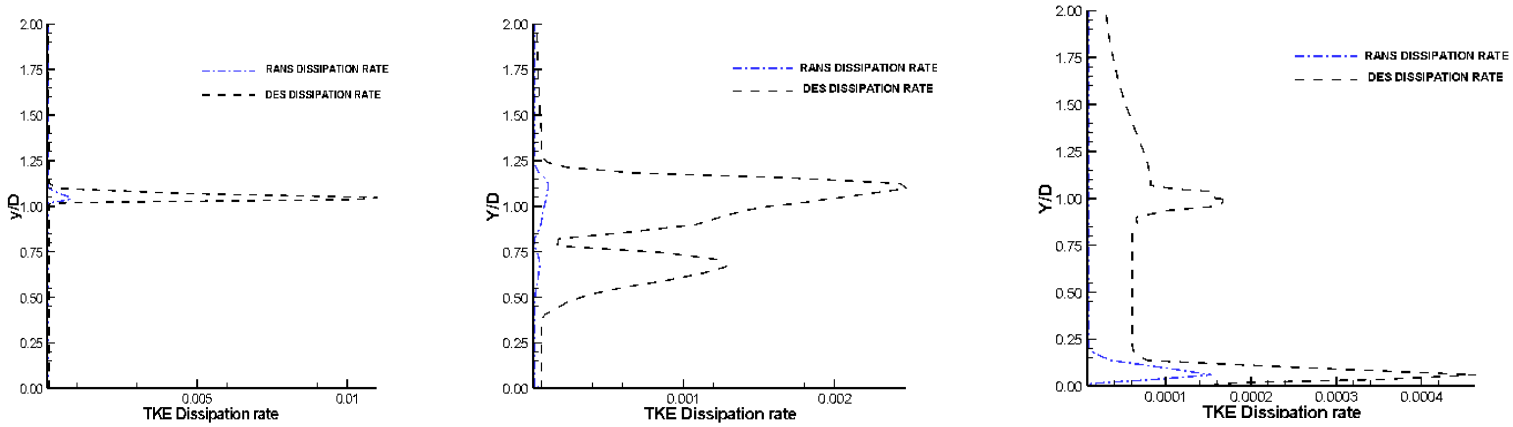

X/L=0.2 X/L=0.5 X/L=0.8

Figure 13 Span-wise averaged time-mean turbulent kinetic energy dissipation rates [ε and $k^{3/2}/(C_b * \Delta)$] profiles (DES1)

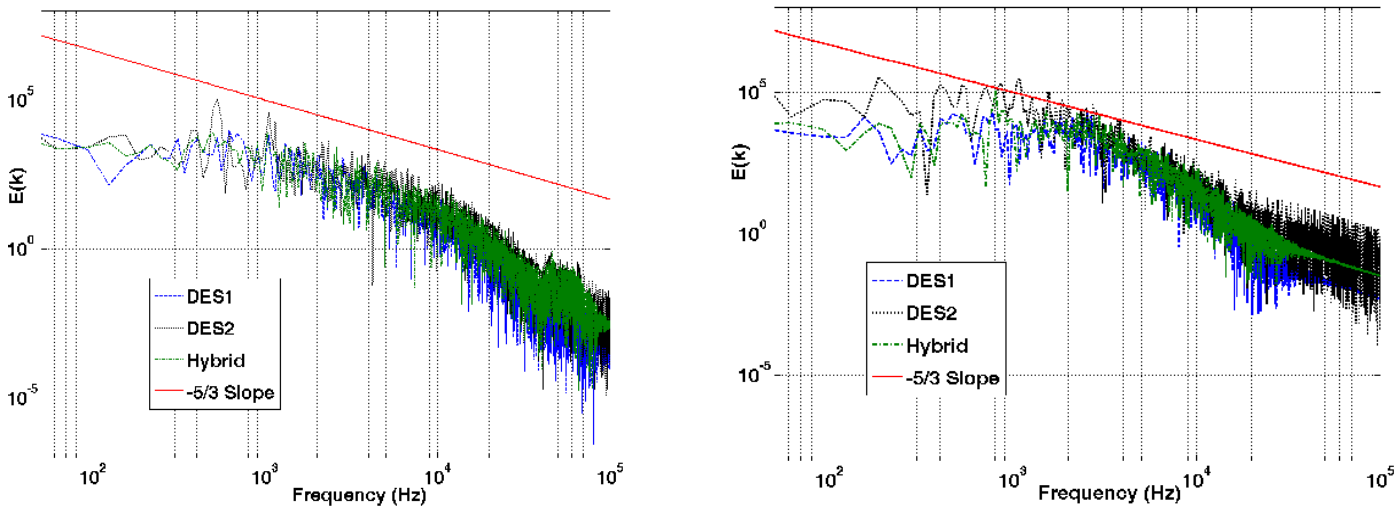

X/L = 0.2 X/L = 0.8

Figure 14 Span-wise averaged grid resolved TKE spectra in the cavity shear layer at cavity opening (Y/D = 1.0)